Showcasing research from Professor Jones' laboratory, Department of Bioengineering, University of Texas, Dallas, U.S.A. Artist is Lei Zhang, Creative Technologies, M.F.A.

Modeling iontophoretic drug delivery in a microfluidic device

We present the first iontophoresis-on-chip (IOC) platform that mimics the outcome of iontophoretic drug delivery for the treatment of breast cancer. The IOC platform and corresponding mathematical model enabled the precise quantification of carboplatin drug delivery and its corresponding anti-cancer efficacy under various voltages and currents. We show that a 50 mV DC electric field and a 3 mA electrical current significantly increased drug delivery and tumor cell death (MDA-MB-231 triple-negative breast cancer cells). The IOC platform and drug delivery model are promising tools for precise delivery of chemotherapeutics into solid tumors.

ROYAL SOCIETY
OF **CHEMISTRY**

rsc.li/loc

Modeling iontophoretic drug delivery in a microfluidic device†

Maryam Moarefian,[a] Rafael V. Davalos, [iD][b] Danesh K. Tafti,[a]
Luke E. Achenie[c] and Caroline N. Jones [iD]‡*[de]

Iontophoresis employs low-intensity electrical voltage and continuous constant current to direct a charged drug into a tissue. Iontophoretic drug delivery has recently been used as a novel method for cancer treatment *in vivo*. There is an urgent need to precisely model the low-intensity electric fields in cell culture systems to optimize iontophoretic drug delivery to tumors. Here, we present an iontophoresis-on-chip (IOC) platform to precisely quantify carboplatin drug delivery and its corresponding anti-cancer efficacy under various voltages and currents. In this study, we use an *in vitro* heparin-based hydrogel microfluidic device to model the movement of a charged drug across an extracellular matrix (ECM) and in MDA-MB-231 triple-negative breast cancer (TNBC) cells. Transport of the drug through the hydrogel was modeled based on diffusion and electrophoresis of charged drug molecules in the direction of an oppositely charged electrode. The drug concentration in the tumor extracellular matrix was computed using finite element modeling of transient drug transport in the heparin-based hydrogel. The model predictions were then validated using the IOC platform by comparing the predicted concentration of a fluorescent cationic dye (Alexa Fluor 594®) to the actual concentration in the microfluidic device. Alexa Fluor 594® was used because it has a molecular weight close to paclitaxel, the gold standard drug for treating TNBC, and carboplatin. Our results demonstrated that a 50 mV DC electric field and a 3 mA electrical current significantly increased drug delivery and tumor cell death by 48.12% ± 14.33 and 39.13% ± 12.86, respectively ($n = 3$, p-value < 0.05). The IOC platform and mathematical drug delivery model of iontophoresis are promising tools for precise delivery of chemotherapeutic drugs into solid tumors. Further improvements to the IOC platform can be made by adding a layer of epidermal cells to model the skin.

1. Introduction

Intravenous chemotherapy is the traditional method for administering cytotoxic agents to cancer patients. Unfortunately, the full potential of anti-cancer drugs is limited because of systemic toxicity and poor tumor perfusion. In an attempt to improve the efficacy of anti-cancer drugs while mitigating their side effects, many groups have reported on the clinical use of electric fields to improve drug delivery. Most studies focus on the electropermeabilization of cells *via* high-intensity electric fields.[1–7] More recently, however, the use of iontophoresis *via* low intensity electric fields[8] was reported in animal models[9–13] and in humans.[14–17] Iontophoresis enhances drug delivery by electrophoresis, the movement of charged drug molecules in the tumor's extracellular matrix surrounding tumor capillaries. During cancer treatment, iontophoretic devices with external power and drug flow controls are implanted proximal to the tumor or onto the skin of the patient.[17–19] However, iontophoretic delivery of chemotherapeutic drugs into the tumor microenvironment is still not well-defined.[20,21] After passing the epidermis, iontophoresis enhances drug delivery *via* three mechanisms in the tumor vasculature (Fig. 1): 1) the electric field and current drives ions through the endothelial membrane of the blood vessels; 2) the ion-electric field interaction provides electrophoretic movement of ions, which increases ion

[a] *Department of Mechanical Engineering, Virginia Polytechnic Institute and State University, Blacksburg, VA 24061, USA*

[b] *Department of Biomedical Engineering and Mechanics, Virginia Polytechnic Institute and State University, Blacksburg, VA 24061, USA*

[c] *Department of Chemical Engineering, Virginia Polytechnic Institute and State University, Blacksburg, VA 24061, USA*

[d] *Department of Biological Sciences, Virginia Polytechnic Institute and State University, Life Sciences 1 Bldg., Rm. 221, 970 Washington Street SW, Blacksburg, VA 24061, USA*

[e] *Department of Bioengineering, The University of Texas, Dallas, TX, 75080, USA*

† Electronic supplementary information (ESI) available. See DOI: 10.1039/d0lc00602e

‡ Current address: The University of Texas at Dallas Bioengineering and Sciences Building, 12.806, 800 N Loop Rd, Richardson, TX 75080 Caroline. Jones@UTDallas.edu
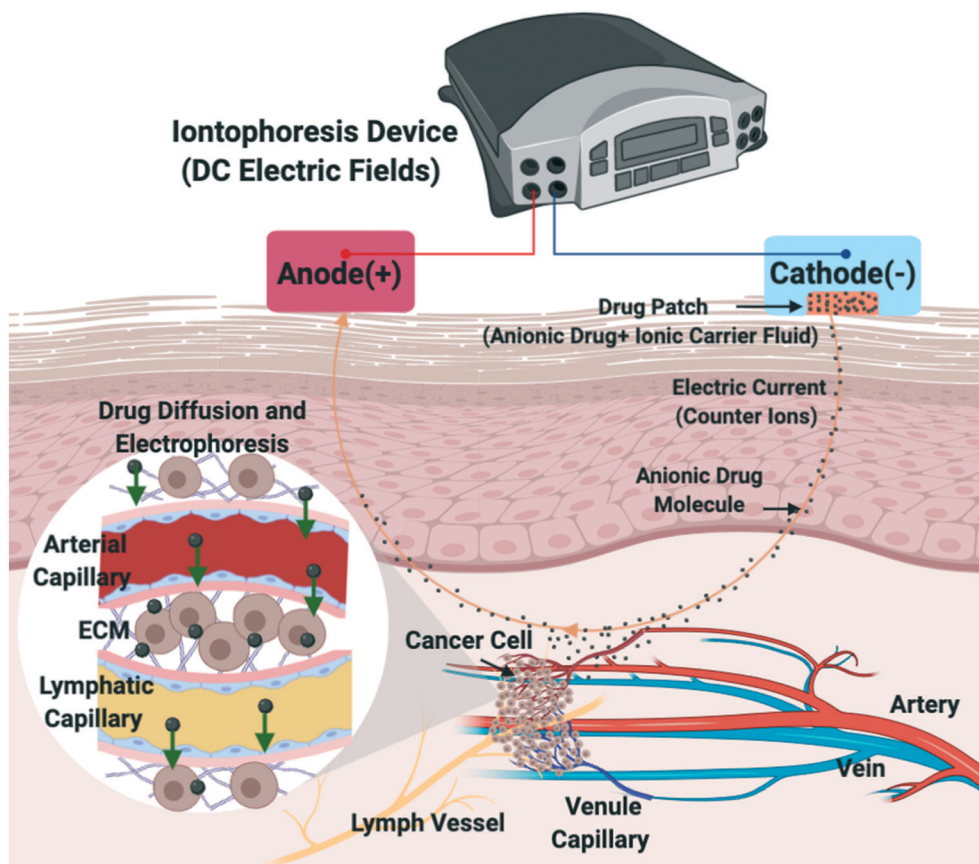
Fig. 1 Iontophoretic transdermal drug delivery into the tumor vasculature *in vivo*. The schematic shows the *in vivo* transport of an anionic drug from the artery to the tumor where it eventually drains into the lymph vessel. Iontophoretic transdermal drug delivery includes insertion of the cathode along with the drug patch on the skin from where the anionic drug molecules move to the tumor facilitated by the transport of the counter ions (from carrier solvent) to the anode.

delivery out of the blood vessel; and 3) electroosmotic flow produces bulk motion of the solvent itself, which carries ions or neutral species within the solvent 'stream'.[19,22] To date, most *in vitro*[21,23–26] and *in vivo*[27,28] studies focused on overcoming human epidermal membrane (HEM) drug resistance by using iontophoresis with a short delivery duration of the electric field. There is a need, however, to precisely control and predict the rate, direction, and distance of drug delivery in the tumor extracellular matrix (ECM) when using iontophoresis techniques. After passing through the HEM, iontophoretic drug delivery is still blocked by the ECM. Physiological and biological barriers within the ECM not only decrease the efficacy of chemical compounds, but also delay the compounds from reaching tumor cells in concentrations sufficient enough to exert a therapeutic effect.[14,17] Barriers to iontophoretic drug delivery created by the ECM is a critical issue that must be addressed. Using a diffusion-based model, our groups has previously[29] described that a 70% porosity, heparin-based hydrogel was a biomimetic scaffolding for modeling the chemoresistance of MDA-MB-231 triple-negative breast cancer (TNBC) ECM.[29] Therefore, we chose to use a heparin-based hydrogel with 70% porosity to represent the ECM of an *in vivo* tumor.[30,31]

Previous microfluidic *in vitro* studies have been conducted to mimic the three-dimensional microenvironments of tumors using on-chip technologies including the tumor vasculature network, which promotes drug resistance in the tumor microenvironment. Recent studies have utilized microfluidic platforms to obtain further insights into the mechanisms of electric field stimulation on cancer cells in 3D as well as the specific parameter values that affect tumor growth but do not harm surrounding, non-cancerous cells present in the tissue.[32] The microfluidic approach facilitates numerous advantages including: (1) the precise control of the biomaterials' physical and chemical properties to resemble the physiological ECM; (2) nanoliter volumes reduce reagent usage and facilitates reproducibility;[33] and (3) controlling the physics of drug transport phenomena in the presence of an applied electric field aids in the design and testing of new therapeutic approaches.[34–36]

In silico simulations are well-suited for testing combinations of multiple physical laws (*e.g.*, diffusion and electrophoresis) and are used for estimating drug concentration profiles in the tumor.[37–39] However, the fundamental mathematical model that incorporates the physics of electrophoresis transport is not well-defined.

Based on the work of Pascal et al.,[40] it was demonstrated in their electrokinetics drug delivery model[41] that the application of an electric field enhances drug delivery at both micro- and macro-scales. However, a validated electrokinetics model[42] that can be used for the prediction of the tumor response to chemotherapy in the presence of an applied low-intensity DC electric field has not been reported.

To address these issues, we developed both iontophoresis-on-chip (IOC) platform and mathematical model of iontophoretic drug delivery. Our iontophoresis-on-chip (IOC) platform allows for three unique applications: (1) acupuncture electrodes facilitate electrode insertion into the microfluidics and precise control over the location and direction of the applied electric field. (2) Incorporation of heparin-based hydrogels into fluidic channels to mimic and precisely control the physiology of the tumor ECM.[43–51] (3) The open microfluidic platform facilitates exchange of the cell medium so as to maintain a constant pH and expose cancer cells to a drug of interest up to 48 h after 3D cell culture. Our mathematical model enabled us to predict optimal parameters (electric field intensity, direction), which were then validated in vitro. Our iontophoresis-on-chip (IOC) platform is the first microfluidic system in the literature to offer the opportunity to investigate the effects of electrophoretic carboplatin delivery into TNBC cells (MDA-MB-231) that are encapsulated in a heparin-based hydrogel.

2. Materials and methods

2.1. Design and fabrication of the microfluidic iontophoresis platform

The iontophoresis-on-chip (IOC) platform was designed to mimic tumor vasculature by providing a top layer of arterial capillaries and two side channels of lymph capillaries in the bottom layer (Fig. 2A). The heparin-based hydrogel and cell culture medium (DMEM/F-12 + 10% FBS) is found between the top and the bottom layers and plays the role of a salt bridge. Sterile stainless-steel acupuncture needles with a diameter of 0.12 mm (Kingli, China) were used as electrodes to construct the DC electric field circuit (Fig. 2B and C). The negative electrode was placed in the top layer and the positive electrodes were placed in the inlet and outlet of the bottom layer's hydrogel channel (Fig. 2A and B). The master mold was patterned using two layers of photoresist: (i) the first layer (i.e., the top layer) consists of a central well (1.5 mm wide and 3 mm thick) and has the role of supplying media to cells that are encapsulated in hydrogel in the bottom layer; (ii) the second layer (i.e., the bottom layer) consists of a cell culture chamber that has the dimensions of 3×3 mm^2, two sink channels with the dimensions of 0.5×3 mm^2, 15 ports with the dimensions of 0.15×0.15 mm^2 between the cell culture chamber and each sink channel, and two side hydrogel channels with the dimensions of 0.5×5 mm^2 (Fig. 2A). The thickness of the
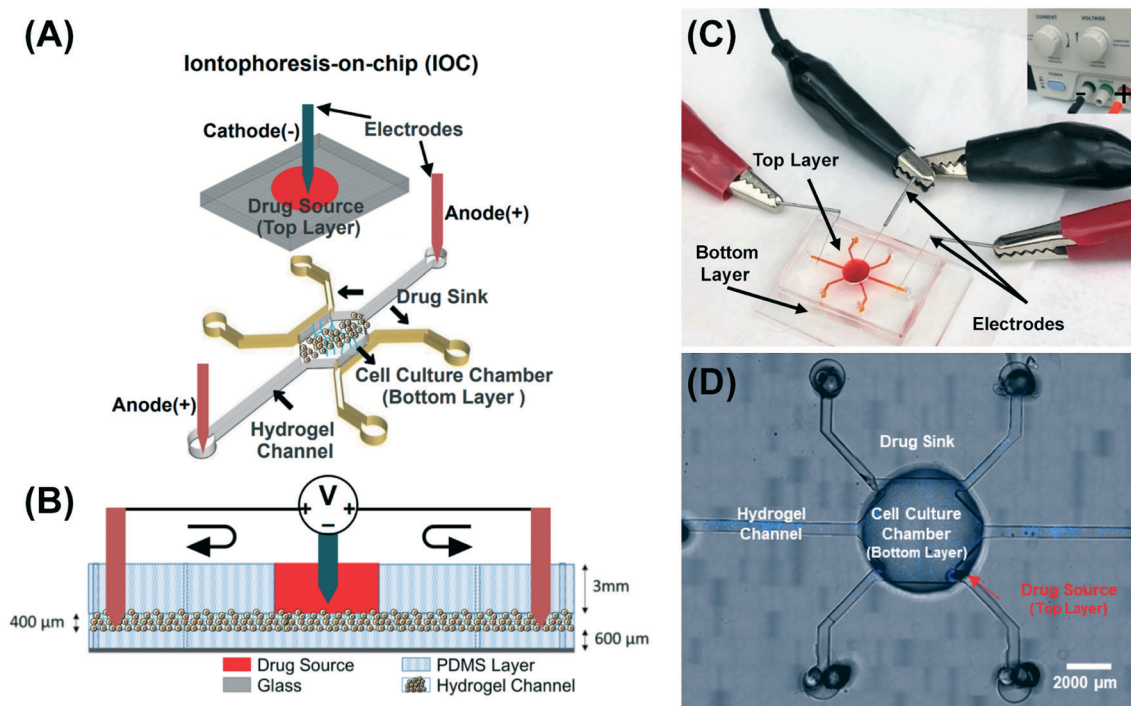
Fig. 2 Iontophoresis-on-chip (IOC) for quantifying iontophoretic delivery of chemotherapeutic drugs in vitro. (A) Microfluidic experiment setup, three-dimensional top view of microfluidic device, negative electrode inserted in drug source well and positive electrodes added to the bottom tumor region layer. (B) Side view of the open microfluidic device and the electric field circuit. (C) Image of experimental setup and application of a DC electric field for drug delivery from the top layer into the tumor region in the bottom layer. (D) Microfluidic device designed to measure iontophoresis drug delivery. Bottom layer includes: 1) drug sink. 2) Cell culture chamber for MDA-MB-231 cells (blue, Hoechst stain). 3) Electrophoresis channels for the delivery of drugs from the cell culture chamber to the side channels through electrophoresis and diffusion. Top layer is the drug source.

bottom layer was optimized to 400 μm using the SU8-2100 photoresist and was fabricated according to the manufacturer's (MicroChem Corp.) instructions. Microfluidic devices were produced by replica molding using polydimethylsiloxane, (PDMS, Sylgard 184; Ellsworth Adhesives, Wilmington, MA, USA) on the master wafer, and fabricated using standard microfabrication techniques.[52] We aligned and bonded the two PDMS layers of the microfluidic platform using a Nikon SMZ-1 stereo microscope and a Nordson MARCH (AP-300) oxygen plasma bonder, respectively. After bonding the two layers, the inlets and outlets were punched using a 0.75 mm biopsy puncher (Fig. 2D). Finally, a 6-well glass-bottom plate (MatTek, Ashland, MA, USA) was plasma-treated along with the PDMS IOC devices and the devices were bonded to the plate using a hot plate (85 °C for 10 min).

2.2. Hydrogel preparation and dose response curve

The HyStem-HP Hydrogel Kit w/ PEGSSDA (ESI BIO GS315P) was used to prepare the heparin hydrogel. The kit is composed of lyophilized solids of Heprasil® (thiol-modified sodium hyaluronate with thiol-modified heparin), Gelin-S® (thiol-modified gelatin), and PEGSSDA™ (disulfide containing polyethylene glycol di-acrylate), as well as degassed deionized water (DG Water). Gels were prepared as per manufacturer's directions. Cell seeding density and drug concentration optimization experiments were done in 384 well-plates with a 0.06 cm^2 growth area, which is approximately the growth area of the fabricated microfluidic device (0.09 cm^2). The drug was applied after 48 h of incubation. Cells were stained using a live and dead cell fluorescent assay (Abcam, Cambridge, MA) after 72 h of incubation. Dose–response curves of paclitaxel (Sigma-Aldrich, St. Louis, MO) and carboplatin (Sigma-Aldrich, St. Louis, MO) were obtained in single cells using a 10 K cell density in 30 μL of heparin-hydrogel. The paclitaxel dose response curve showed that 11 nM was the 90% effective dose (EC_{90}) and the carboplatin dose response curve showed that 12 nM of carboplatin killed the maximum fraction of cells (85%) (Fig. S1A†). Because of these dose response curves, we chose to use 2 nM of the drugs to use doses less than the EC_{90} for both paclitaxel and carboplatin in the microfluidic *in vitro* environment. We tested the effect of electric field on the delivery of paclitaxel and carboplatin separately to examine this effect on both charged (carboplatin) and neutral (paclitaxel) drug delivery.

2.3. Cell culture and iontophoresis-on-chip (IOC) assay

The human TNBC cells used in this study were from an invasive ductal carcinoma cell line (MDA-MB-231, American Type Cell Culture HTB-26). Gibco™ Dulbecco's modified Eagle's medium F-12 (DMEM/F-12), containing high levels of glucose and GlutaMAX™ supplemented with 10% (v/v) fetal bovine serum (FBS, ATCC, Manassas, VA) and 1% (v/v) penicillin–streptomycin (100 units per mL penicillin and 0.1 mg per mL streptomycin), was used as a complete culture medium for the TNBC cells. The encapsulated breast cancer cells were studied using heparin hydrogel in complete media

(DMEM + 10% FBS + 1% P/S). The cells were suspended in the Heprasil and Gelin-S mixture before adding the PEGSSDA crosslinker at a density of 10 K single cells in 30 μL of hydrogel. 2 nM concentrations of paclitaxel and carboplatin were used because they kill approximately 71% of cells without an applied electric field (Fig. S1A†). We used cells on top of the gel, and encapsulated cells inside the gel for 3D cell culture in the microfluidic device. The encapsulated cells in the hydrogel were introduced into the device through manual injection using a syringe and tubing until a uniform distribution of cells was attained in the cell culture chamber. In our study, we set the flow rate to zero (eliminating electroosmotic flow) and focused on electrophoresis transport only. To model the iontophoresis, we needed to define: 1) ECM porosity; 2) drug concentration; 3) cell density; and 4) drug charge. We set the drug concentration to be less than the effective dose of 90% (ED_{90}), which we measured in both standard well plates and in the microfluidic device (Fig. S1†). Application of an external electric voltage resulted in faster delivery of anionic drugs compared to cationic drugs.[35] We compared an anionic drug,[53,54] carboplatin, to the gold standard non-ionized drug, paclitaxel. We also studied TNBC cells cultured in heparin-based hydrogel as a tumor ECM biomaterial.[29,55] In our device, we validated the application of a 50 mV electric field to an ECM of 70% porosity to increase drug delivery to a tumor's single cells. We also varied the drug type (charge). In this study, we controlled low-intensity DC electric fields for electrophoretic drug delivery in the tumor's single cells. We quantified the effect of a 50 mV DC electric field and a 3 mA electric current on the percent of dead cells both mathematically and experimentally using a mass transfer model and a microfluidic platform, respectively. Our IOC mimics the tumor extracellular matrix through the use of MDA-MB-231 single cells in a heparin-based hydrogel, the lymph capillary (drug sink), and the blood capillary (drug source). We initially used a physics based mathematical model[41] for sensitivity analysis and parameter optimization to reduce the number of *in vitro* experiments. To experimentally prove the chosen electric field intensity of 50 mV derived from the sensitivity analysis, we showed the effect of electrophoresis transport on increasing ionic macromolecule delivery in heparin-based hydrogel.

The experiment was conducted for a total of 72 h where the cells were initially seeded and allowed to grow for 48 h and then treated with 2 nM of the drug and 50 mV of electric field for 5 h. The electric field was discharged after 5 h, however, the cells were left in the drug solution for an additional 19 h. Finally, the cells were stained with live and dead cell fluorescent assay medium (Abcam, Cambridge, MA) after 72 h (Fig. S3†).

2.4. Electrokinetics and mass transfer model

To reduce the number of *in vitro* experiments, we employed a physics-based model to predict the minimum electric field intensity needed to affect the maximum

fraction of cells killed by simulating the effect of iontophoresis on carboplatin delivery. The model was then validated with a biomimetic three-dimensional microfluidic experiment by comparing the measured and predicted percentage of dead cells. See the ESI† for a more detailed description of the coupled electrokinetics and mass transfer model.

### 2.5. Drug delivery model optimization and sensitivity analysis

Sensitivity analysis was used to eliminate a trial and error approach for determining the electric field intensity when conducting the IOC experiments. Sensitivity analysis of the electric field potential, between 0 and 70 mV, at the blood vessel wall showed 43.01 mV as the optimum electric field intensity to obtain a 79% cell death rate (Fig. 3B).

Three non-dimensional numbers and the electric potential in the tumor region were optimized using GRG (generalized reduced gradient) nonlinear solver.[56] The optimal value of φ_2 (electric field intensity), 43.01 mV, was instrumental in eliminating multiple microfluidic *in vitro* experiments for electric field intensity optimization. Tables S1 and S2† show the dependent and independent variables, their sensitivity ranges, and optimum value to obtain the maximum fraction of cells killed.

2.6. Transport of macromolecules into heparin-based hydrogel

The first experimental setup was used to determine the ionized fluorescent dye concentration with and without
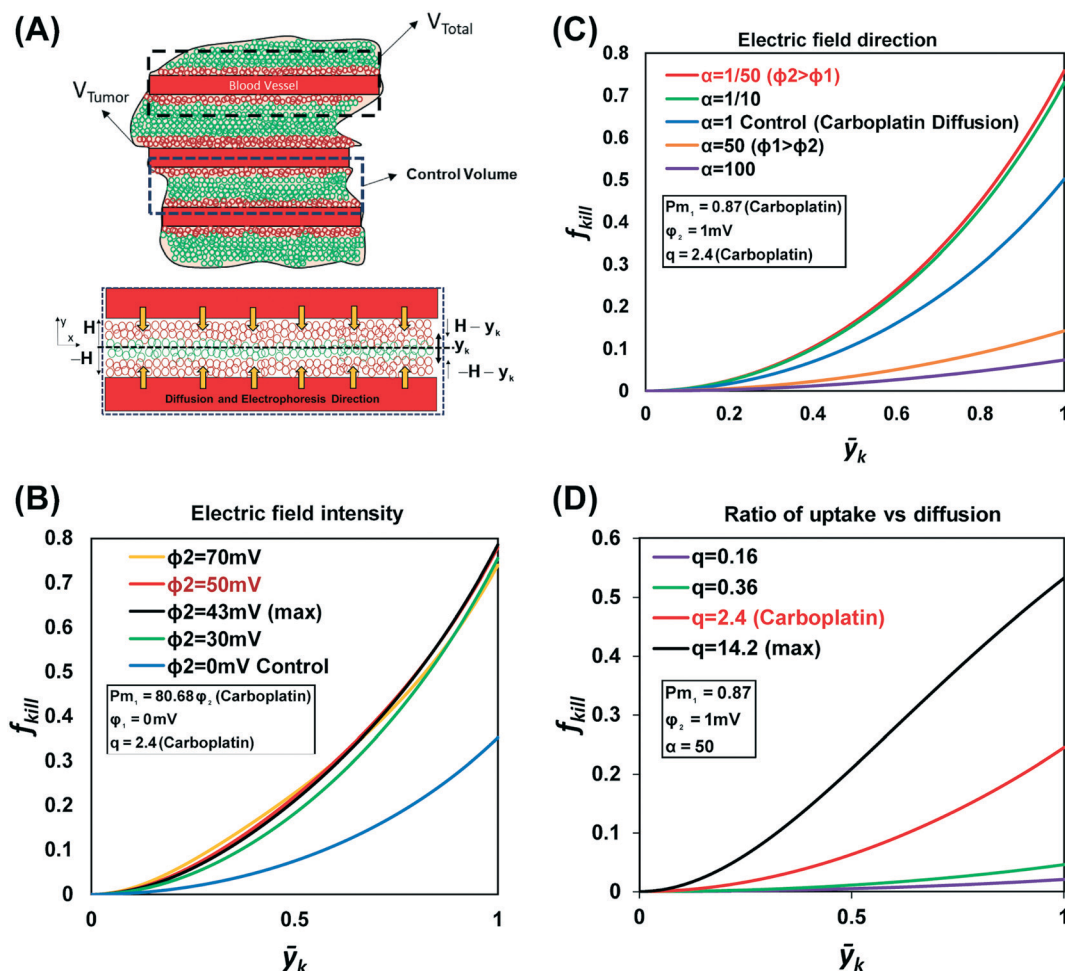
Fig. 3 Mathematical model sensitivity analysis of the fraction of tumor cells killed model. (A) The schematic illustrates the volume of the analytical domain under study (V_{Total}), which is the sum of the volume of a single blood vessel and the surrounding tumor mass (V_{Tumor}). V_{Tumor} includes both the live and dead tumor cells, represented by the green and red circles, respectively. $V_{control}$ depicts the volume between two consecutive blood vessels and is used as the control volume for the mathematical model, with idealized system boundaries (H, $-H$, $H - y_k$, $-H - y_k$). (B) The graph shows the variation in the fraction of tumor cells killed (f_{kill}) over a dimensionless kill distance y_k, for different values of Pm_1 and electric field intensities. The sensitivity analysis predicted 43 mV as the optimal electrical voltage required to maximize the fraction of tumor cells killed (0.79). (C) The graph shows the variation in the fraction of tumor cells killed (f_{kill}) over a dimensionless kill distance, y_k, for different values of α (which is the ratio of electric potential in the drug source (φ_1) to the electric potential in the tumor (φ_2)). When φ_2 is 50 times more than φ_1, the diffusion and electrophoretic movement of the charged drug molecules are in the same direction, and the fraction of tumor cells killed is at its maximum (0.75). (D) The graph shows the variation in the fraction of tumor cells killed (f_{kill}) over a dimensionless kill distance, y_k, for different values of q (the ratio of the drug uptake rate to the drug diffusion). For carboplatin $q = 2.4$, where the fraction of cells killed is 0.25.

applying a 50 mV of DC electric field. Sensitivity analysis and model optimization show that the electric potential of 43.01 mV resulted in the maximum fraction of tumor cells killed. Due to the restriction in the precision of our DC power supply (DC power supply must be >10 mV), we had to choose between 40 mV and 50 mV. We loaded a heparin-based hydrogel in the bottom layer, closed the outlets to eliminate gravitational flow, placed the device under a Nikon TiE time lapse microscope, and allowed the hydrogel to solidify (10–15 min). 30 μL of dye was added to the top layer and live imaging was started simultaneously. Live images were taken every 1 minute for 5 h in two 1 mm^2 x–y planes in the central chamber and the hydrogel channel over a 1.2 mm distance. The fluorescence intensity was measured over 10 different depths (40 μm) within the hydrogel (400 μm). The average intensity was determined over the 1 mm^2 x–y plane. The final average intensity is the average of x–y plane intensities at 10 different hydrogel depths. The calibration curve was used (Fig. S2†) to convert average dye intensity to dye concentration. We used Alexa Fluor 594® fluorescent dye with a molecular weight of 819.85 g mol^{-1}, which is similar to paclitaxel's molecular weight (853.91 g mol^{-1}) and close to carboplatin molecular weight (371.25 g mol^{-1}). The experimental result of Alexa Fluor 594® concentration *versus* time validated the finite element model of dye concentration (diffusion and electrophoresis delivery with 50 mV electric potential gradient) in the porous hydrogel region.

2.7. Confocal microscopy and image processing

Confocal microscopy was used to measure the fraction of cells killed with and without applying a 50 mV DC electric field. A confocal microscope (ZEISS LSM 880 with Airyscan) fitted with a ZEISS Axiocam 503 mono camera and a computerized stage was used to take fluorescent images. The microscope was controlled using ZEN software (Carl Zeiss Microscopy GmbH, Germany). Images were processed using ImageJ (NIH, Bethesda, MD). To calculate the fraction of cells killed (or the percentage of dead cells), the fluorescent light intensities from tetramethyl rhodamine iso-thiocyanate (TRITC, red: dead cells) were divided by the total fluorescent light intensities from TRITC (red: dead cells) and fluorescein isothiocyanate (FITC, green: live cells) in each 10 μm plane along the hydrogel's z-axis. Results from the confocal images were used for validation of the fraction of cells killed model[41] (Fig. 6C).

2.8. Microfluidics *in vitro* experiment statistical analysis

Statistical analyses were performed using Prism version 8.1.2 (332) software (GraphPad Software, La Jolla, CA) with a confidence level of $\alpha = 0.05$. Two-way analysis of variance (ANOVA) was used to test for differences in the number of dead cells after electrophoresis treatment ($n = 3$) in our microfluidic device ($n = 3$). When results of ANOVA were significant, Tukey *post hoc* comparisons were used to examine differences among treatment groups. Data are presented as the arithmetic mean ± SD.

3. Results and discussion

The combined mathematical and experimental approach in our study included four steps. First, we used a physics-based mathematical model,[41] sensitivity analysis, and parameter optimization to eliminate trial and error in conducting *in vitro* experiments to determine the optimal electric voltage. Second, we showed the effect of electrophoresis transport on cationic macromolecule concentration (Alexa Fluor 594®) in the porous region (heparin-based hydrogel) using a transient electrokinetics drug release computational model, which was validated by a microfluidic *in vitro* experiment. Third, the IOC device was used to study carboplatin and paclitaxel delivery to TNBC cells in an *in vitro* experiment using 50 mV of electric field (EF) and 3 mA of electric current. Fourth, the *in vitro* experimental results were used to validate the fraction of cells killed in the mathematical model.

3.1. Drug delivery mathematical model optimization and sensitivity analysis

The physics-based model development is shown in the ESI.† In the final fraction of tumor killed function, eqn (24),† three non-dimensional numbers relate to the physics of uptake, diffusion, and electrophoresis drug transport and needed to be analyzed. Pm_1 is the ratio between the electric potential and diffusivity, q is the ratio between the uptake rate of the carboplatin and diffusivity, and α is the ratio of electric potential in the drug source to the electric potential in the tumor. Three non-dimensional numbers and the electric potential in the tumor region were optimized using GRG (generalized reduced gradient) nonlinear solver.[56]

The first non-dimensional number, $Pm_1 = \frac{zF\mu\varphi_2}{2D}$, is the ratio between the electric potential and the diffusion coefficient. We consider the problem of maximizing the fraction of cells killed subject to varying non-dimensional numbers. The Pm_1 number is the function of the electric potential in the tumor region. Except for φ_2, other terms in Pm_1 are constant properties of carboplatin. We only look at the carboplatin property because it is a charged drug candidate for studying the effect of electric field on its delivery. At a large Pm_1 (3.47), the electric potential φ_2 has the highest value (43.01 mV); therefore, the fraction of cells killed is maximized (0.79) (Fig. 3B). Our results show the positive effect that electric potential has on the fraction of cells killed and that it can overcome carboplatin's low diffusion coefficient. As Pm_1 decreases, the fraction of cells killed also decreases due to a decrease in φ_2. When Pm_1 is zero, the result indicates the fraction of cells killed (0.37) without applying an electric field.

The direction of electrophoresis can be opposite the direction of drug diffusion. The second non-dimensional number is α, which is the ratio of electric potential in the drug source to the electric potential in the tumor. The fraction of cells killed decreases when α is close to 1, *i.e.*, when there is no electric potential gradient. Therefore, when

$\alpha = (\varphi_1 = \varphi_2)$ the fraction of cells killed is minimized (0.44) (Fig. 3C). As α increases ($\varphi_1 > \varphi_2$), the electrical potential gradient is in the opposite direction of the concentration gradient, so the fraction of cells killed decreases. Note that α = 1/50 means φ_2 is 50 times more than φ_1, at which point the fraction of cells killed is maximized (0.79).

The non-dimensional number is analyzed to examine the fraction of cells killed based on drug uptake rate and diffusion. q is the ratio of the drug uptake rate to drug diffusion. Since q is always positive, the model always increases (monotonic) with different values of positive q. At small q values (0.16), carboplatin diffusion dominates over the uptake rate. High carboplatin diffusion can occur due to a decrease in the tumor drug uptake rate. Therefore, the number of cells killed at high carboplatin uptake (q = 14.2) leads to a maximized fraction of cells killed (0.55) and a decrease in tumor drug resistance (Fig. 3D).

When q is 2.4 for carboplatin, the uptake rate of carboplatin is smaller than its diffusion where the fraction of tumor cells killed is 0.25. The fraction of cells killed reaches an asymptote by increasing the value of q, which depends on the properties of the drug. Therefore, applying an electric field to enhance chemotherapy delivery of carboplatin is essential to kill the maximum fraction of cells (0.79). The graph shows that the primary sources of uncertainty in percent dead cells are the

drug uptake rate and diffusivity, and this type of sensitivity analysis allows drug designers to assess the effects of the physical properties of the drugs in the interest of building robust drug delivery models. Our model investigated diffusion and electrophoresis drug transport into single cells. Increasing the electric field intensity increases the fraction of cells killed; however, the new physics of transport, such as joule heating and electroosmotic flow, should be added to the model for a more accurate prediction.

3.2. Delivery of cationic fluorescent dye into the hydrogel using a low intensity electric field

Sensitivity analysis and electric potential gradient optimization showed that an electric potential of 43.01 mV resulted in the maximum fraction of tumor cells being killed (0.7–0.8 or 70–80%). Based on mathematical model sensitivity analysis, we used a 50 mV electric field intensity for drug delivery experiments on single cells. Because of the restriction in the precision of our DC power supply (DC power supply must be >10 mV), we had to choose 50 mV instead of 43.01 mV. To test our hypothesis using a 50 mV electric field in transient condition, finite element modeling of macromolecule transport in hydrogel was computed. The model was validated with an electrophoresis microfluidic
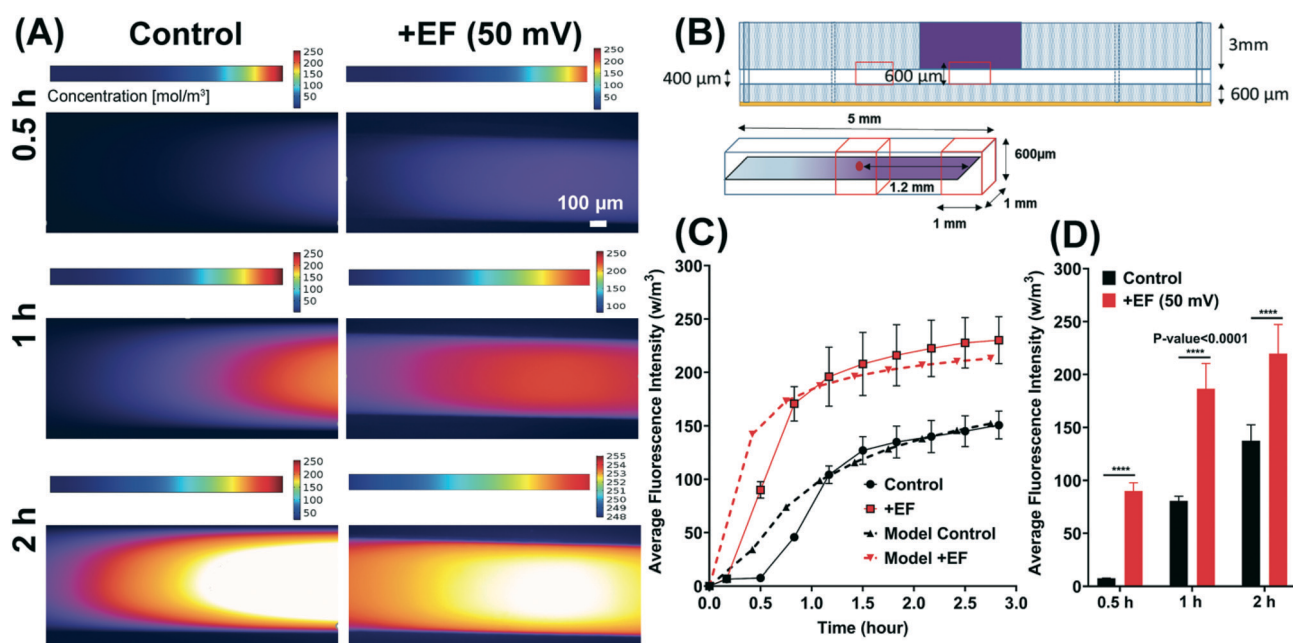
Fig. 4 Low-intensity electric fields increase cationic macromolecule transport into the hydrogel. (A) Snapshots comparing the transient concentration of the Alexa Fluor 594® dye in the hydrogel channel at 0.5 h, 1 h, and 2 h time points under the following conditions: left: diffusion only (top: finite element model result, bottom: experimental result); right: diffusion and electrophoresis at 50 mV electric fields (top: finite element model result, bottom: experimental result). (B) Representation of the regions in the cell culture chamber and the hydrogel channel of the device, for the measurement of dye transient concentration (top: experimental regions, bottom: computational domain). (C) The graph shows the validation of finite element model results for the dye transient concentration obtained experimentally by measuring average fluorescence intensity in the hydrogel channel under the following conditions: (i) control (diffusion only), (ii) diffusion and electrophoresis at 50 mV electric fields. (D) Summary of the average fluorescence intensity of Alexa Fluor 594® dye at 0.5 h, 1 h, and 2 h time points under the same conditions as C. Graph show an increase (48.12%, n = 46, p-value <0.0001) in the average fluorescence intensity of the dye by applying 50 mV of electric potential gradient in the hydrogel microchannel after 2 h.

experiment using the IOC device by comparing the measured and predicted normalized fluorescence intensity of the dye. Alexa Fluor 594® cationic dye diffusion and electrophoretic delivery were investigated in a 3 h experiment and a transient continuum mass transfer model. The regions in the cell culture chamber and hydrogel channel of the device for the measurement of dye transient concentration (top: experimental regions, bottom: computational domain) are shown in Fig. 4B. The *in silico* simulation and *in vitro* experiment showed an increase (48.12%, $n = 46$, p-value <0.0001) in the average fluorescence intensity of the dye by applying 50 mV electric potential gradient in the hydrogel

microchannel (Fig. 4A, C and D). The finite element model of the concentration profile in the microchannel was validated with an *in vitro* experiment of Alexa Fluor 594® cationic dye diffusion and electrophoretic delivery (Fig. 4C).

3.3. A low-intensity electric field increases carboplatin delivery in breast cancer single cells

Based on model sensitivity analysis (section 3.2), we specified the low-intensity electric field to be 50 mV. Drug concentration optimization (Fig. S1A†) showed that 2 nM of paclitaxel and carboplatin have around a 59% and 71% tumor cell death rate,
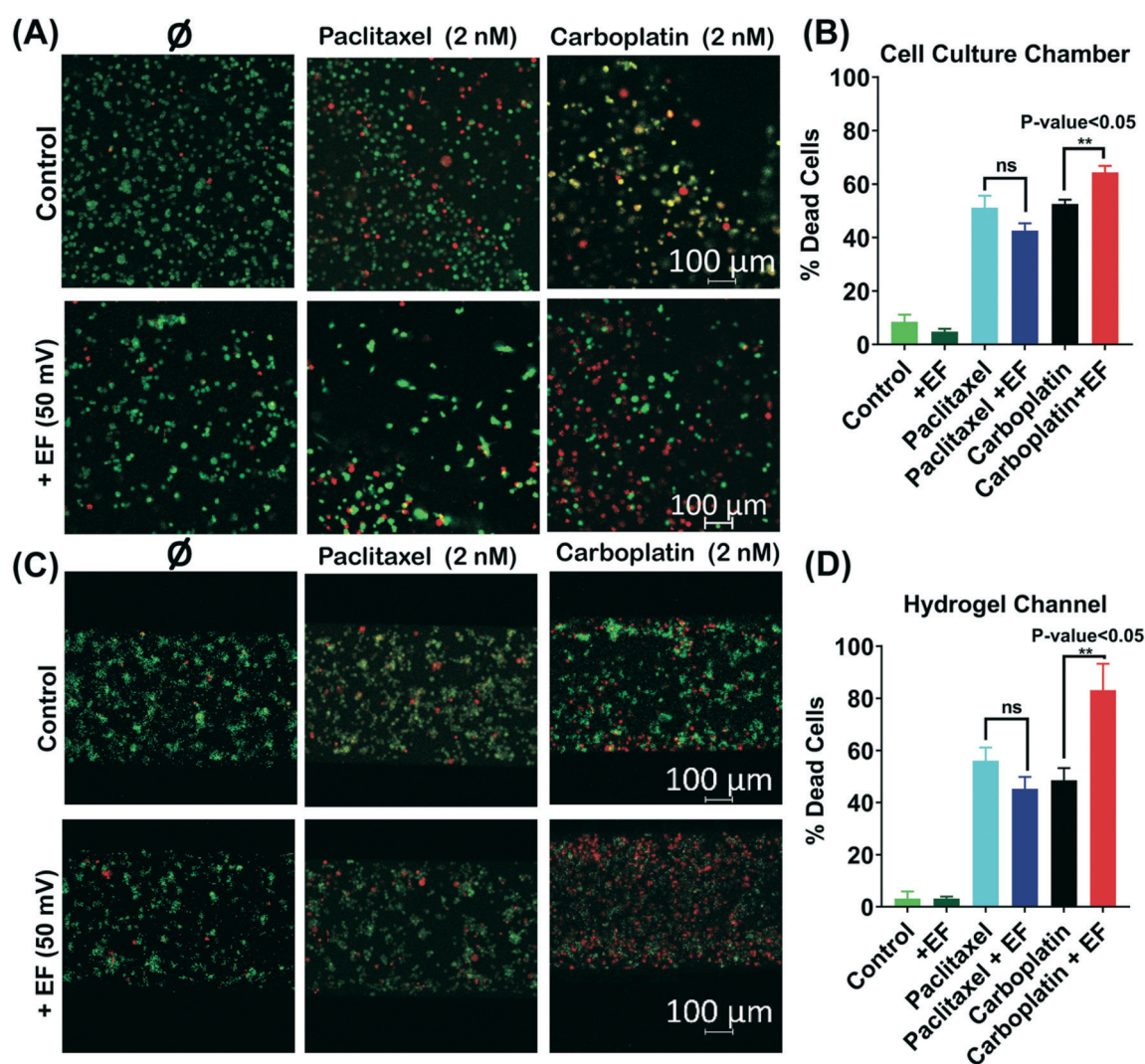
Fig. 5 Low-intensity electric fields increase the delivery of carboplatin to single tumor cells. Confocal microscope images showing the live-dead cell staining of single tumor cells when exposed to the following treatments: cell culture medium, DMEM/F-12 (no drug); 2 nM of paclitaxel (non-ionized drug); and 2 nM of carboplatin (anionic drug), with and without 50 mV of electric field in the device's (A) cell culture chamber and (C) hydrogel channel. Graph shows the percent dead tumor cells when exposed to the six following treatments: (1) control (bright green): cell culture medium, DMEM/ F-12 (no drug, no electric field), (2) +EF (dark green): cell culture medium, DMEM/F-12 (no drug, with 50 mV of electric field), (3) Paclitaxel (bright blue): 2 nM of paclitaxel (non-ionized drug, no electric field), (4) Paclitaxel+EF (Dark blue): 2 nM of paclitaxel (non-ionized drug, with 50 mV of electric field), (5) Carboplatin (black): 2 nM of carboplatin (anionic drug, no electric field), and (6) Carboplatin+EF (red): 2 nM of carboplatin (anionic drug, with 50 mV of electric field), in the device's (B) cell culture chamber and (D) hydrogel channel, respectively. Tumor cells that are treated with 2 nM of carboplatin in the presence of 50 mV electric field showed the least viability of all the treatments, with dead cell percent about 64% ($n = 3$, p <0.05) in cell culture chamber and 83% ($n = 3$, p <0.05) in hydrogel channel.

respectively. Therefore, we specified operating at 2 nM drug concentrations, which is less than the EC_{90} (effective concentration for 90% of the cells being dead). A significant difference was observed in the percent of dead cells by applying a 50 mV electric field and 3 mA electric current for 3 h (Fig. 5A and C). The percent of dead cells increased by 22% ($n = 3$, p-value <0.05) in the cell culture chamber (Fig. 5B) and 39% ($n = 3$, p-value <0.05) in the hydrogel channel (Fig. 5D).

3.4. Fraction of cells killed model validation with *in vitro* experiment

The "fraction of cells killed" model was developed to facilitate the prediction of the iontophoresis outcome. The *in vitro* results of percent dead cells *versus* hydrogel depth were used for model validation (Fig. 6A). A summary of results of the percent of dead cells at different distances from the bottom of the chamber shows an increase in percent dead cells when delivering carboplatin using electrophoresis (Fig. 6B). The validated fraction of cells killed model shows

an increase in the percent of dead cells when applying a 50 mV electric field and 3 mA electric current for 3 h experimentally and mathematically (Fig. 6C).

Our results demonstrate that 50 mV of DC electric field and 3 mA of electric current increases drug delivery by 48.12% and increases cell death by 39.13%. Our obtained experimental results validated our recent drug transport model.[41]

The correlation between the fraction of cells killed model and the *in vitro* experiment was measured using two different methods (Table S3†):[57] 1. RNMSE (root normalized mean square error) and 2. FB (fraction of bias). The correlation between cationic dye concentration in hydrogel experimental and theoretical values was calculated using the same methodologies. We found that the FB (fractional bias) value was equal to 0.02, where a positive FB indicated that the model is under prediction, and an RNMSE (root normalized mean square error)[54] equal to 0.3 indicated low scattering from the mean. Overall, the statistical analysis indicated a strong correlation between the model and the microfluidic experiment.
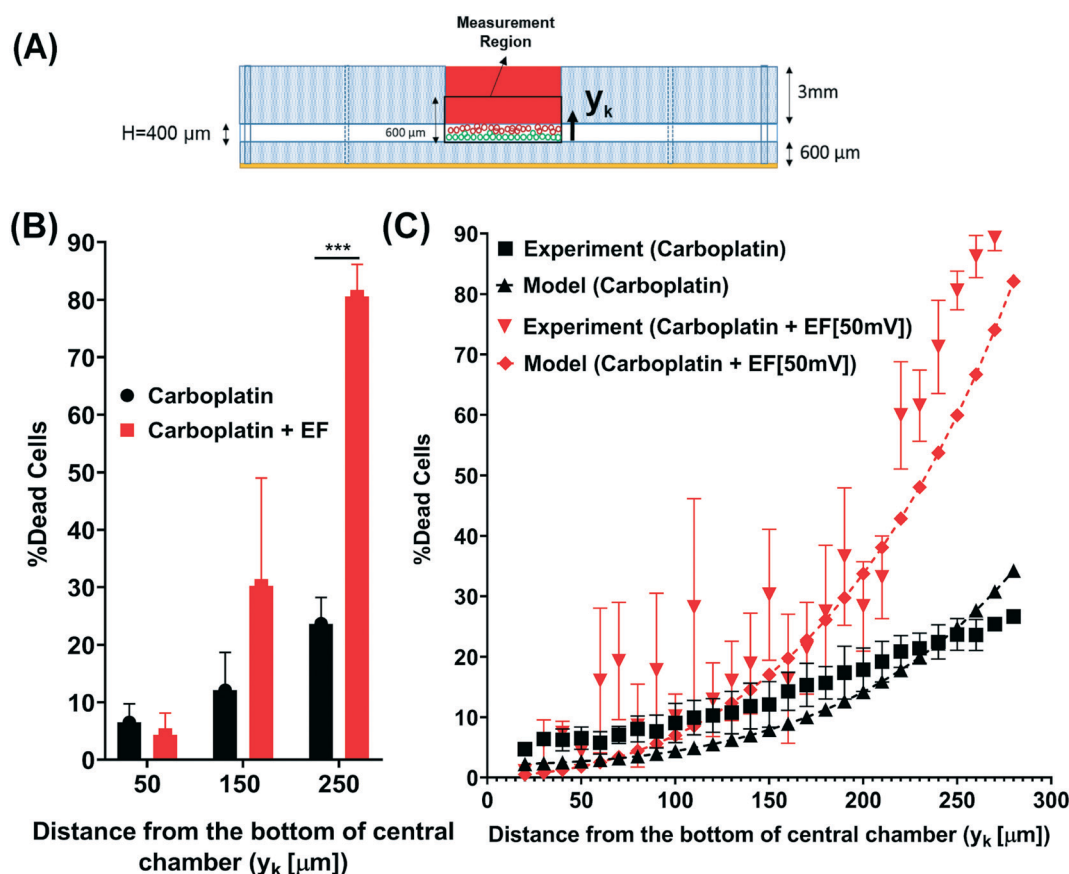

Fig. 6 Percent dead tumor cells model validation shows that low-intensity electric field promotes iontophoretic delivery of carboplatin into breast cancer cells. (A) Representative of the experimental measurement region in the cell culture chamber of the device, for calculating the percent dead tumor cells when treated with 2 nM of carboplatin with and without 50 mV of electric field. (B) Graph shows increase in percent dead tumor cells that are seeded at 50 μm, 150 μm, and 250 μm distance from the bottom of the cell culture chamber and treated with 2 nM of carboplatin with and without 50 mV of electric field; the difference in the percent dead cells when treated with 2 nM of carboplatin with electric field is significantly higher at 250 μm (closest to drug source) compared to other distances. (C) Percent dead tumor cells model validation with the *in vitro* experiment shows an accurate correlation between model and experiment (Table S3†).

4. Conclusion

This paper demonstrates, for the first time, an iontophoresis-on-chip platform that mimics the outcome of iontophoretic drug delivery for the treatment of breast cancer. The mathematical model for the carboplatin concentration profile between two blood vessels in a confined tumor volume was able to accurately predict our *in vitro* microfluidic results. In this study, we varied the drug type (charge) and cell density as the two main parameters for the on-chip experiments. As expected, iontophoresis was only effective in increasing the charged drug (carboplatin) delivery to the individual tumor cells. Our device could potentially be used for high-throughput screening of charged drug candidates for iontophoretic treatment for breast cancer. Our modeling and experimental results show that an applied electric field intensity of 50–70 mV of DC electric fields and 3 mA of electric current led to the maximum percentage of dead cells (70–90%). This low intensity electric field has been reported to have minimal side effects on healthy tissues and is significantly lower than that following electroporation. The on-chip platform allows us to precisely control the physics of transport phenomena by adjusting the device geometries, boundary conditions, and initial values of drug dose and electric field intensity to match the mathematical model. The predictive models that we developed in this manuscript define the influence of DC electrical fields and electric current on iontophoretic drug delivery to tumors and may possibly assist physicians in designing an effective treatment regimen for breast cancer patients.[58] We proved the synergy between our mathematical models and our *in vitro* experiments, which led to a reduction in the number of electric field intensity trials using the mathematical model sensitivity analysis. We then proved the accuracy of the chosen electric field intensity values from the sensitivity analysis by macromolecule electrophoretic delivery into the heparin-based hydrogel microfluidics experiment. The results of the macromolecule electrophoresis delivery into the porous hydrogel was used to validate a transient electrokinetics mass transfer model.

In the future, our device also has the capability to vary flow, ECM porosity, electric field intensity, tumor size, and tumor type. This model is the first step towards generating a predictive model for *in vivo* applications. Further improvements to the model for transdermal iontophoretic drug delivery can be made and validated by adding additional components in the microfluidic device, mimicking the human epidermis. Currently, iontophoresis is only used for transdermal drug delivery to accessible tumors. In the future, endoscopic surgeries may enable the implantation of 3D printed hydrogels and electrodes[59–62] for electrically-controlled drug delivery into inaccessible solid breast tumors.

5. Author contributions

MM, and CNJ designed the experiments and device, conceived the experiment(s), edited the manuscript, and the work was done under CNJ's supervision. MM designed iontophoresis-on-chip, conducted the experiments, developed the electrokinetics models, and analyzed the data. DKT, RVD, and LEA contributed to the microfluidic device design and computational model. All authors have read and approved the article.

6. Funding

Conflicts of interest

There are no conflicts to declare.

Acknowledgements

References

1 E. Neumann, *et al.*, Gene transfer into mouse lyoma cells by electroporation in high electric fields, *EMBO J.*, 1982, **1**(7), 841.

2 M. Okino and H. Mohri, Effects of a high-voltage electrical impulse and an anticancer drug on *in vivo* growing tumors, *Jpn. J. Cancer Res.*, 1987, **78**(12), 1319–1321.

3 S. Orlowski, *et al.*, Transient electropermeabilization of cells in culture: increase of the cytotoxicity of anticancer drugs, *Biochem. Pharmacol.*, 1988, **37**(24), 4727–4733.

4 G. Sersa, *et al.*, Electrochemotherapy in treatment of tumours, *Eur. J. Surg. Oncol.*, 2008, **34**(2), 232–240.

5 M. Wichtowski, *et al.*, Electrochemotherapy in Breast Cancer - Discussion of the Method and Literature Review, *Breast Care*, 2017, **12**(6), 409–414.

6 M. G. Bourke, *et al.*, Effective treatment of intractable cutaneous metastases of breast cancer with electrochemotherapy: Ten-year audit of single centre experience, *Breast Cancer Res. Treat.*, 2017, **161**(2), 289–297.

7 M. Wichtowski, *et al.*, Electrochemotherapy in the Treatment of Breast Cancer Metastasis to the Skin and Subcutaneous Tissue - Multicenter Experience, *Oncol. Res. Treat.*, 2019, **42**(1–2), 47–51.

8   A. K. Banga, S. Bose and T. K. Ghosh, Iontophoresis and electroporation: comparisons and contrasts, *Int. J. Pharm.*, 1999, **179**(1), 1–19.

9   A. Banerjee, *et al.*, Intestinal iontophoresis from mucoadhesive patches: a strategy for oral delivery, *J. Controlled Release*, 2019, **297**, 71–78.

10 L. F. Dalmolin and R. F. V. Lopez, Nanoemulsion as a Platform for Iontophoretic Delivery of Lipophilic Drugs in Skin Tumors, *Pharmaceutics*, 2018, **10**(4), 214.

11 H. Liang, *et al.*, Effects of methycobal iontophoresis combined with balance acupuncture on peripheral facial paralysis, *Zhongguo Zhenjiu*, 2018, **38**(9), 955–960.

12 M. J. Pikal, The role of electroosmotic flow in transdermal iontophoresis, *Adv. Drug Delivery Rev.*, 2001, **46**(1), 281–305.

13 S. R. Patel, *et al.*, *In vitro* and *in vivo* evaluation of the transdermal iontophoretic delivery of sumatriptan succinate, *Eur. J. Pharm. Biopharm.*, 2007, **66**(2), 296–301.

14 J. D. Byrne, J. J. Yeh and J. M. DeSimone, Use of iontophoresis for the treatment of cancer, *J. Controlled Release*, 2018, **284**, 144–151.

15 J. B. Sloan and K. Soltani, Iontophoresis in dermatology: a review, *J. Am. Acad. Dermatol.*, 1986, **15**(4), 671–684.

16 J. D. Byrne, *et al.*, Impact of formulation on the iontophoretic delivery of the FOLFIRINOX regimen for the treatment of pancreatic cancer, *Cancer Chemother. Pharmacol.*, 2018, **81**(6), 991–998.

17 J. D. Byrne, *et al.*, Local iontophoretic administration of cytotoxic therapies to solid tumors, *Sci. Transl. Med.*, 2015, **7**(273), 273ra14.

18 J. B. Wolinsky, Y. L. Colson and M. W. Grinstaff, Local drug delivery strategies for cancer treatment: Gels, nanoparticles, polymeric films, rods, and wafers, *J. Controlled Release*, 2012, **159**(1), 14–26.

19 T. Karpiński, Selected Medicines Used in Iontophoresis, *Pharmaceutics*, 2018, **10**(4), 204.

20 E. Eljarrat-Binstock and A. J. Domb, Iontophoresis: A non-invasive ocular drug delivery, *J. Controlled Release*, 2006, **110**(3), 479–489.

21 E. Eljarrat-Binstock, *et al.*, *In Vitro* and *In Vivo* Evaluation of Carboplatin Delivery to the Eye Using Hydrogel-Iontophoresis, *Curr. Eye Res.*, 2008, **33**(3), 269–275.

22 B. J. Kirby, *Micro-and nanoscale fluid mechanics: transport in microfluidic devices*, Cambridge university press, 2010.

23 S. K. Li, *et al.*, *In vitro* and *in vivo* comparisons of constant resistance AC iontophoresis and DC iontophoresis, *J. Controlled Release*, 2003, **91**(3), 327–343.

24 J.-P. Sylvestre, R. H. Guy and M. B. Delgado-Charro, *In Vitro* Optimization of Dexamethasone Phosphate Delivery by Iontophoresis, *Physical Therapy*, 2008, **88**(10), 1177–1185.

25 E. Eljarrat-Binstock, *et al.*, Charged nanoparticles delivery to the eye using hydrogel iontophoresis, *J. Controlled Release*, 2008, **126**(2), 156–161.

26 E. Eljarrat-Binstock, *et al.*, Methylprednisolone delivery to the back of the eye using hydrogel iontophoresis, *J. Ocul. Pharmacol. Ther.*, 2008, **24**(3), 344–350.

27 H.-Z. Jia and X.-J. Peng, Efficacy of iontophoresis-assisted epithelium-on corneal cross-linking for keratoconus, *International Journal of Ophthalmology*, 2018, **11**(4), 687–694.

28 J. H. Jung, *et al.*, Ocular drug delivery targeted by iontophoresis in the suprachoroidal space using a microneedle, *J. Controlled Release*, 2018, **277**, 14–22.

29 N. Menon, H. X. Dang, U. S. Datla, M. Moarefian, C. B. Lawrence, C. A. Maher and C. N. Jones, Heparin-based hydrogel scaffolding alters the transcriptomic profile and increases the chemoresistance of MDA-MB-231 triple-negative breast cancer cells, *Biomater. Sci.*, 2020, **8**(10), 2786–2796.

30 P. Karuppuswamy, *et al.*, Functionalized hybrid nanofibers to mimic native ECM for tissue engineering applications, *Appl. Surf. Sci.*, 2014, **322**, 162–168.

31 Q. L. Loh and C. Choong, Three-dimensional scaffolds for tissue engineering applications: role of porosity and pore size, *Tissue Eng., Part B*, 2013, **19**(6), 485–502.

32 A. Pavesi, *et al.*, Engineering a 3D microfluidic culture platform for tumor-treating field application, *Sci. Rep.*, 2016, **6**, 26584.

33 I. C. Lee, Cancer-on-a-chip for Drug Screening, *Curr. Pharm. Des.*, 2018, **24**(45), 5407–5418.

34 S. Murdan, Electro-responsive drug delivery from hydrogels, *J. Controlled Release*, 2003, **92**(1), 1–17.

35 M. Curcio, *et al.*, On demand delivery of ionic drugs from electro-responsive CNT hybrid films, *RSC Adv.*, 2015, **5**(56), 44902–44911.

36 S. M. Rahman, J. M. Campbell, R. N. Coates, K. M. Render, C. E. Byrne, E. C. Martin and A. T. Melvin, Evaluation of intercellular communication between breast cancer cells and adipose-derived stem cells *via* passive diffusion in a two-layer microfluidic device, *Lab Chip*, 2020, **20**(11), 2009–2019.

37 J. Aroesty, *et al.*, Tumor growth and chemotherapy: Mathematical methods, computer simulations, and experimental foundations, *Math. Biosci.*, 1973, **17**(3–4), 243–300.

38 J. Siepmann and F. Siepmann, Modeling of diffusion controlled drug delivery, *J. Controlled Release*, 2012, **161**(2), 351–362.

39 C. Mircioiu, *et al.*, Mathematical Modeling of Release Kinetics from Supramolecular Drug Delivery Systems, *Pharmaceutics*, 2019, **11**(3), 140.

40 J. Pascal, *et al.*, Mechanistic patient-specific predictive correlation of tumor drug response with microenvironment and perfusion measurements, *Proc. Natl. Acad. Sci. U. S. A.*, 2013, **110**(35), 14266–14271.

41 M. Moarefian and J. A. Pascal, Fundamental mathematical model shows that applied electrical field enhances chemotherapy delivery to tumors, *Math. Biosci.*, 2016, **272**, 1–5.

42 J. H. Sung, C. Kam and M. L. Shuler, A microfluidic device for a pharmacokinetic–pharmacodynamic (PK–PD) model on a chip, *Lab Chip*, 2010, **10**(4), 446–455.

43 M. F. McGuire, *et al.*, Formalizing an Integrative, Multidisciplinary Cancer Therapy Discovery Workflow, *Cancer Res.*, 2013, **73**(20), 6111.

44 H. Enderling and K. A. Rejniak, Simulating Cancer: Computational Models in Oncology, *Front. Oncol.*, 2013, **3**, 233.

45 S. C. Choe, *et al.*, Model for *in vivo* progression of tumors based on co-evolving cell population and vasculature, *Sci. Rep.*, 2011, **1**, 31.

46 H. B. Frieboes, *et al.*, Physical Oncology: A Bench-to-Bedside Quantitative and Predictive Approach, *Cancer Res.*, 2011, **71**(2), 298.

47 C. Liu, *et al.*, Use of mathematical models to understand anticancer drug delivery and its effect on solid tumors, *Pharmacogenomics*, 2011, **12**(9), 1337–1348.

48 F. Michor, *et al.*, What does physics have to do with cancer?, *Nat. Rev. Cancer*, 2011, **11**, 657.

49 H. M. Byrne, Dissecting cancer through mathematics: from the cell to the animal model, *Nat. Rev. Cancer*, 2010, **10**, 221.

50 A. Swierniak, M. Kimmel and J. Smieja, Mathematical modeling as a tool for planning anticancer therapy, *Eur. J. Pharmacol.*, 2009, **625**(1), 108–121.

51 P. Dogra, *et al.*, Mathematical modeling in cancer nanomedicine: a review, *Biomed. Microdevices*, 2019, **21**(2), 40.

52 S. Brittain, *et al.*, Soft lithography and microfabrication, *Phys. World*, 1998, **11**(5), 31.

53 A. J. Di Pasqua, *et al.*, Activation of Carboplatin by Carbonate, *Chem. Res. Toxicol.*, 2006, **19**(1), 139–149.

54 A. Ciancetta, C. Coletti, A. Marrone and N. Re, Activation of carboplatin by carbonate: A theoretical investigation, *Dalton Trans.*, 2012, **41**(41), 12960–12969.

55 M. Kim, *et al.*, Heparin-based hydrogel as a matrix for encapsulation and cultivation of primary hepatocytes, *Biomaterials*, 2010, **31**(13), 3596–3603.

56 L. S. Lasdon, R. L. Fox and M. W. Ratner, Nonlinear optimization using the generalized reduced gradient method. Revue française d'automatique, informatique, recherche opérationnelle, *Oper. Res.*, 1974, **8**(V3), 73–103.

57 M. Soni, *et al.*, A performance evaluation of WRF model using different physical parameterization scheme during winter season over a semi-arid region, India, *International Journal of Earth and Atmospheric Science*, 2014, **1**(3), 104–114.

58 A. Calvert, *et al.*, Carboplatin dosage: prospective evaluation of a simple formula based on renal function, *J. Clin. Oncol.*, 1989, **7**(11), 1748–1756.

59 A. Simeunovic and D. J. Hoelzle. Coupled Dynamics of Material Delivery and Robotic Manipulator Axes in *Endoscopic Additive Manufacturing, in 2019 American Control Conference (ACC)*, 2019.

60 A. A. Adib and D. Hoelzle. Hybrid System Model of Microextrusion-Based Direct-Write Additive Manufacturing, in *2019 American Control Conference (ACC)*, 2019.

61 C. J. Bloomquist, *et al.*, Controlling release from 3D printed medical devices using CLIP and drug-loaded liquid resins, *J. Controlled Release*, 2018, **278**, 9–23.

62 H. J. Oh, *et al.*, 3D Printed Absorber for Capturing Chemotherapy Drugs before They Spread through the Body, *ACS Cent. Sci.*, 2019, **5**(3), 419–427.